

Chitin Nanocrystals as an Eco-friendly and Strong Anisotropic Adhesive

Hongzhong Liu, Yue Feng, Xiang Cao, Binghong Luo, and Mingxian Liu*



Cite This: *ACS Appl. Mater. Interfaces* 2021, 13, 11356–11368



Read Online

ACCESS |



Metrics & More



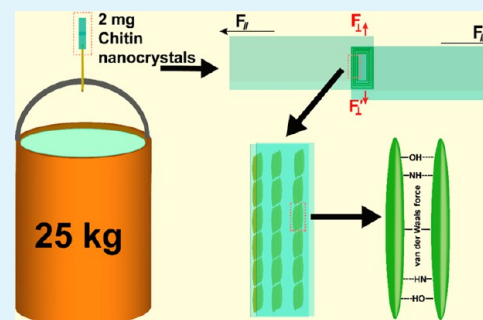
Article Recommendations



Supporting Information

ABSTRACT: To solve the damage to the environment and human body caused by organic solvent adhesives in the utilization process, chitin nanocrystal (ChNC) suspension is explored as a strong anisotropic adhesive, which is an eco-friendly and water-based adhesive with high adhesive strength. ChNCs extracted from crab shells are rod-like nanoparticles with high aspect ratios, which are mainly employed as reinforcing polymer nanocomposites and biomedicine nanomaterials. ChNC suspension sandwiched between substrates forms a long-range ordered superstructure by a self-assembly process. ChNC nanoglue exhibits high anisotropy adhesion strength, i.e., an in-plane shear strength (5.26 MPa) and an out-of-plane shear strength (0.46 MPa) for glass substrates. Moreover, the ChNC nanoglue is suitable to many substrates, such as glass, plastic, wood, metal, paper, etc. The ChNC nanoglue shows high biocompatibility toward the fibroblast cell and rat skin, proving their excellent biosafety. As an eco-friendly and high-performance adhesive, ChNC nanoglue shows promising applications in daily life and industrial fields.

KEYWORDS: chitin nanocrystals, anisotropic adhesive, ChNC nanoglue, biomedicine nanomaterial



ChNC nanoglue shows promising applications in daily life and industrial fields.

INTRODUCTION

Adhesives play a critical role in our daily life such as mending shoes, gluing postage stamps, repairing something, or attaching tags to gifts. With the development of industrialization, a variety of high-performance adhesives have been synthesized. At present, new adhesives have been developed with UV or visual light curing properties, including thermoplastic, rubber, and pressure-sensitive materials.^{1–4} These artificial adhesives usually have high adhesion and strength, but they are not resistant to high temperature. For example, the adhesion provided by commercial 502 cyanoacrylate glue will fail at 150 °C. In addition, they are rarely reusable because of their viscous properties and the surfaces will quickly be contaminated by the adhered materials.⁵ Due to the increasing attentions to environmental problems, the environmental pollution and human health harm brought by the volatile organic compounds (VOCs) from adhesives have become a tricky question. VOCs may have short- and long-term adverse health effects, which include eye, nasal, oral, and lung irritation as well as headaches, nausea, respiratory problems and damage to the liver, kidney, and central nervous system.⁶ For example, the furniture adhesives (phenolic resin, urea formaldehyde resin, and melamine urea formaldehyde resin) would release formaldehyde during the process of use, but formaldehyde is a dangerous genotoxic air pollutant, which is classified as a human carcinogen by the U.S. Environmental Protection Agency.^{7–9} Therefore, it is quite urgent to find a kind of green, eco-friendly, and organic solvent-free glue with high-adhesive strength.

Through self-assembly of nanoparticle suspension in confined space, micro/nanopatterns of the nanoparticles can be formed on glass and other substrates to achieve adhesion.^{10–12} Confined evaporation-induced self-assembly is a common method for studying the assembly behavior of nanoparticles by constructing a narrow space and controlling evaporation of the solvent in it. Fakhruddin et al. used different-curved upper surfaces (a metal sphere, a square cover glass, a round cover glass, and a square pyramid) to form a series of ordered concentric circles by evaporating the suspension of halloysite in a narrow space.^{13,14} The successful assembled superstructure relies on the good dispersion state of the nanoparticles in a solvent, which usually arise from the high surface potentials. Zhao et al. proposed coordination polymer nanoplates as a solid surface adhesive, but the complex synthesis methods and high costs of the nanogluers prevent their further use.¹⁵ Recently, cellulose nanocrystals have also been used as adhesives by a confined evaporation-induced self-assembly process; however, their ultrahigh anisotropic adhesive strength ratios (>70) may hinder its practical application since the adhesion can easily accidentally be broken.¹²

Received: January 29, 2021

Accepted: February 17, 2021

Published: February 26, 2021



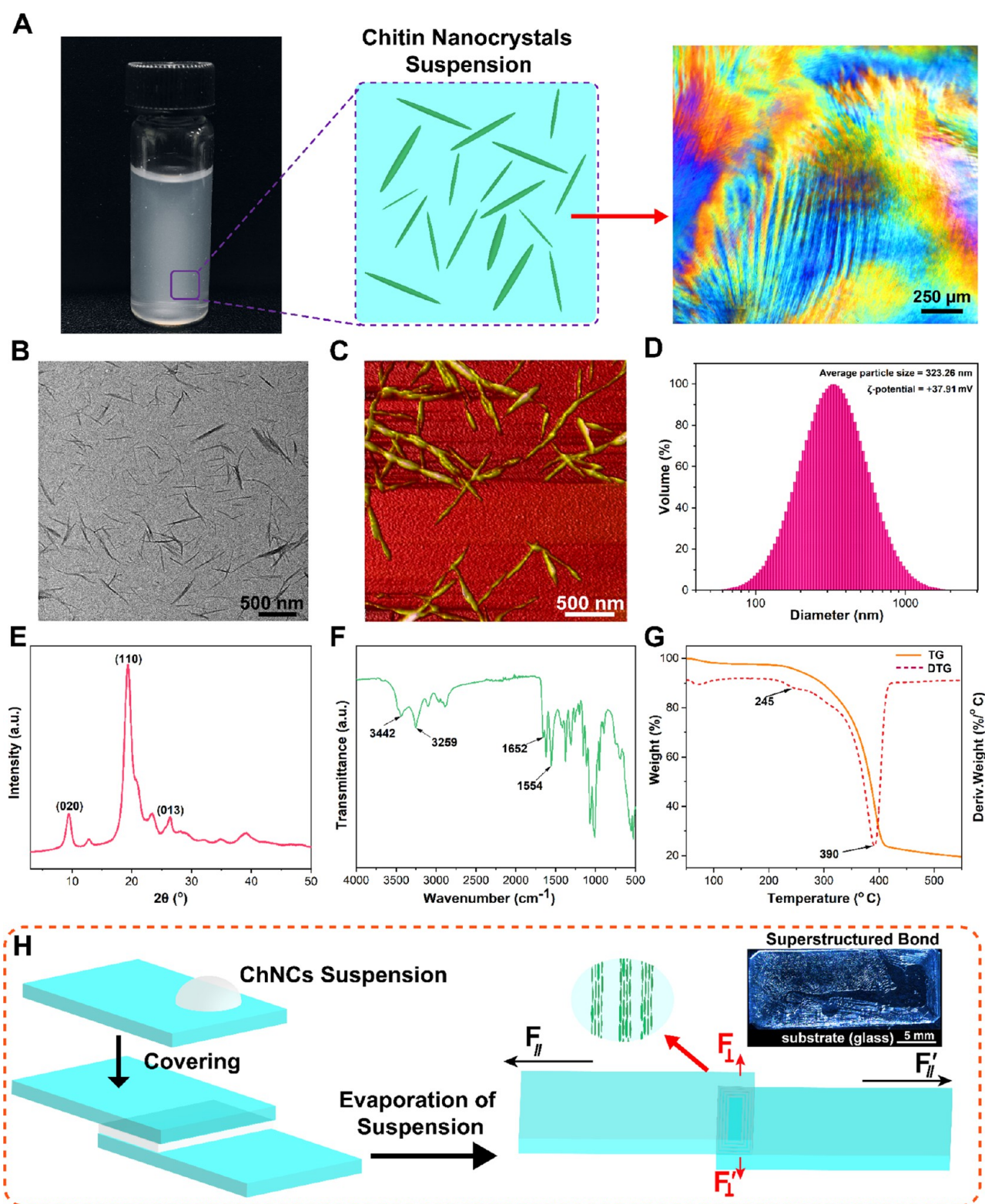


Figure 1. Characterizations of ChNC suspensions. (A) Appearance, structure model, and liquid crystal images. (B) TEM photograph. (C) AFM image. (D) Particle size distribution. (E) XRD pattern. (F) FTIR spectra. (G) TG and DTG curves. (H) Gluing solid surfaces by stacking of ChNC suspensions and the formed superstructure.

Chitin nanocrystals are easily available polysaccharide nanomaterials, which are derived from living organisms such as crabs, shrimps, and insects. Compared with an organic solvent adhesive that emits VOCs, the obvious advantages of ChNCs are biosafety and antibacterial.¹⁶ Chitin is composed of 2-

acetamido-2-deoxy-D-glucose and consists of crystalline and amorphous domains.¹⁷ ChNCs can be obtained by mechanical treatment, acid hydrolysis, and tempo-mediated oxidation to degrade the amorphous domain of chitin.^{18–20} Compared with bulk chitin, ChNCs show a uniform rod-like morphology with a

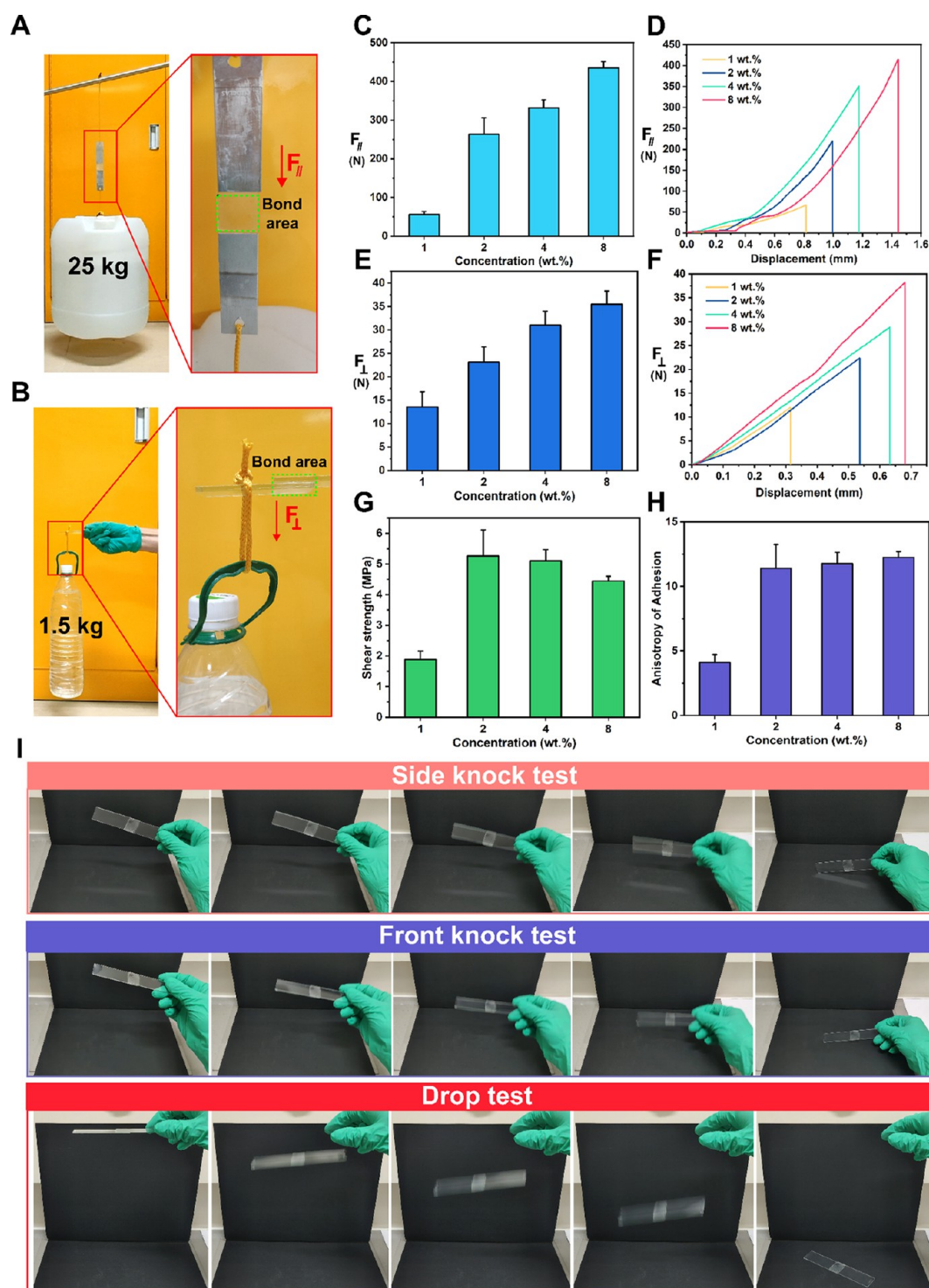


Figure 2. Adhesion properties of ChNC nanoglu. $F_{\parallel} > 250.00$ N load in-plane (A) and $F_{\perp} > 15.00$ N load out-of-plane (B) of ChNC nanoglu hold with objects. In-plane (C, D) and out-of-plane (E, F) load histogram and force–displacement curves of different concentrations of ChNC suspensions. (G) Adhesive shear strength for in-plane lap-shear of different concentrations of ChNC suspensions. (H) Anisotropy of in-plane and out-plane strength as a function of concentrations of ChNC suspensions. (I) The stability test of the bonded glass sheet: side knock test (pink), front knock test (purple), and drop test (red box).

length and width of 200–500 and 15–30 nm, respectively. The aspect ratio of ChNCs is in the range of 5–15,^{21,22} which is one of the key factors for the formation of chiral nematic liquid crystals. Rod-like ChNCs also have a high specific surface area (~ 130 m²/g) and a large number of hydrogen bonds on the surface, which makes the network structure between adjacent ChNCs to have a tendency to form.^{23,24}

In this study, ChNC suspension was sandwiched between two substrates to form a highly ordered layered structure by the evaporation-induced self-assembly process. The rod-like nanoparticles have good contact with the substrate surfaces inducing strong interparticle adhesion, while they stack on each other to form a lamellar structure facilitating a strong cohesion effect. The ChNC nanoglu is applicable to different substrates such as

glass, plastic, wood, metal, paper, etc. ChNC nanoglue has good biocompatibility toward cells and tissues, and the solvent used is water rather than an organic solvent, which shows that the adhesive is safe and reliable for human and environment.²⁵ As a kind of green and environment-friendly adhesive without an organic solvent, ChNC nanoglue has great potentials in daily life and industrial fields.

RESULTS AND DISCUSSION

Characterization of ChNCs. ChNC powder was prepared from crab shells by acid hydrolysis, and ChNC suspension was dispersed homogeneously by ultrasound treatment (Figure 1A and Figure S1A). ChNC suspension (0.05 wt %) was used for morphology analysis and particle size distribution determination. The morphology of ChNCs was characterized by TEM and AFM (Figure 1B,C). ChNCs show a uniform rod-like structure with length and width ranges of 200–500 and 15–30 nm, respectively. The aspect ratio of ChNCs is in the range of 5–15. These results are consistent with a previous study.²⁶ It should be noted that the size of ChNCs is closely related to the acidolysis time and source of chitin.²³ The size distribution of the ChNC suspension is shown in Figure 1D. The main distribution of the particle size ranged from 200 to 600 nm with an average particle size of 323.26 nm. The ζ potential of the ChNCs was determined as +37.91 mV, which ensures the high stability of the suspension. The data obtained from the particle size distribution are consistent with those observed on the morphology. ChNCs display a uniform size and high aspect ratio, which are beneficial to the orientation and formation of nematic liquid crystals of ChNCs in the suspension. The long-range ordered structure formed by the subsequent evaporation self-assembly of ChNCs is an important source of adhesion force, and other types of liquid crystals of nanoparticles are also expected with certain adhesive performance. The positive potential is due to the positive charge of the protonated amino group, which makes the suspension to have good stability and colloidal behavior.²⁶

The XRD pattern of ChNCs is shown in Figure 1E. The typical diffraction peaks of ChNCs are located at 9.3°, 19.1°, and 26.2°, which represent (020), (110), and (013) plane, respectively.²⁷ ChNCs are also studied by FTIR spectra, and characteristic peaks of the ChNCs are observed at 3442 cm⁻¹ (O–H stretching), 3259 cm⁻¹ (N–H stretching), 1652 cm⁻¹ (amide I), and 1554 cm⁻¹ (amide II), suggesting a typical α -chitin structure (Figure 1F).²⁸ The thermal degradation behavior of ChNCs is shown in Figure 1G. ChNCs begin to lose weight under 100 °C due to the loss of adsorbed water, suggesting the hydrophilicity of ChNCs. The initial and maximum degradation temperatures are 245 and 390 °C, respectively. This suggests a high thermal stability of ChNCs, implying that this nanomaterial still maintains its physicochemical performance below 200 °C, which is good for maintaining the adhesive strength at high temperatures.

Herein, based on the characteristics of ChNCs, a highly ordered layered structure was prepared from a drop of ChNC suspension (Figure 1H), which was translated into a highly anisotropic adhesion between solid substrates. A drop of ChNC suspension was sandwiched between two glass sheets to create a confined space. The interparticle water evaporated at 25 °C and 70% relative humidity results in ChNC–ChNC cohesion and a ChNC–substrate adhesion effect, combined with the formation of nematically ordered superstructures (inset in Figure 1H).

Adhesion Properties of ChNC Nanoglue. To demonstrate the adhesion properties of ChNC nanoglue, two glass sheets were glued together by drying the ChNC suspension between them. Interestingly, a 25.0 kg ($F_{\parallel} = 250.00$ N) bucket with water can be easily lifted with the ChNC-glued glass sheet sample (Figure 2A and Movie S1), while the weight of the used ChNCs is only 2.0 mg. This suggests that it has excellent in-plane load capacity. To test the out-of-plane load capacity of the sample, a bottle with 1.5 kg ($F_{\perp} = 15.00$ N) water was held on one side of the glass sheet sample and the other side of the sample was lifted by hand (Figure 2B and Movie S2). The results show that the sample can withstand at least a 1.5 kg out-of-plane load. The excellent adhesion ability of ChNC nanoglue is confirmed by the example of physical loading.

Furthermore, the adhesive properties of the ChNC nanoglue were tested by a universal testing machine. Figure 2C shows that the loading capacity increases with the increase of the ChNC suspension concentration. For the four ChNC concentrations (1, 2, 4, 8 wt %) evaluated, the maximum in-plane loads were 55.60 ± 8.17 , 263.37 ± 42.67 , 364.77 ± 26.77 , and 435.09 ± 15.93 N. Figure 2D shows the load–displacement curves obtained from typical tensile measurements. A load–displacement curve shows a slip–stick behavior, suggesting that the nanocrystals slide at the beginning and then interlock with each other.¹⁵ When the load exceeds a certain value, the adhesion fails immediately. Similarly, the out-of-plane load also increases with the increase of the ChNC concentration, and the maximum out-of-plane load increased from 13.52 ± 3.29 to 23.11 ± 3.25 , to 30.99 ± 3.01 , and 35.51 ± 2.77 N (Figure 2E,F).

It should be noticed that the final adhesive strength of any adhesive depends on the contact areas between the glue and substrates. For the present work, it is not equal for the overlapping area of the two glass sheets and the effective contact area between ChNCs and glass sheets. Therefore, we calculate the effective contact area by analyzing the stereomicroscope images using ImageJ software (Figure S2). The ratio between the contact area and whole overlap increases with the increase of the concentration, although it is not linear. The thickness of the adhesive layer is between 5 and 30 μm . This is from the reason that the increased concentration of ChNC suspension is prior to the increase in both the bonding area and thickness of the adhesive layer rather than solely increasing the bonding area. According to the in-plane load, the adhesive strength values normalized with the contact area were 1.88 ± 0.28 , 5.26 ± 0.85 , 5.1 ± 0.37 , and 4.44 ± 0.16 MPa for ChNC concentrations of 1, 2, 4, and 8 wt %, respectively (Figure 2G, adhesive strength = load / effective contact area, and this calculation method is only used in this part of the discussion). The out-of-plane adhesive strength values were 0.45, 0.46, 0.43, and 0.36 MPa for ChNC concentrations of 1, 2, 4, and 8 wt %, respectively. This results in anisotropy of adhesion for the respective ChNC concentrations of 4.11 ± 0.60 , 11.40 ± 1.85 , 11.77 ± 0.86 , and 12.25 ± 0.45 (Figure 2H). Through the study of adhesion properties of ChNC nanoglue, we found that the lap-shear strength can reach 5.26 MPa, which is comparable to the commercial 502 cyanoacrylate adhesive (~ 8.00 MPa).²⁹

The out-of-plane adhesion developed by evaporation-induced self-assembly based on ChNC suspension in confined space is much smaller than in-plane, and the out-of-plane strength of 2% ChNC nanoglue is only 0.46 MPa. According to the ratio between in-plane and out-of-plane strength values, the anisotropy of adhesive strength is 11.40 ± 1.85 . Compared with other adhesives (Figure S3), ChNC nanoglue has both

sufficient adhesive strength and suitable anisotropy (too small to be used, too large will lead to unstable adhesion), which is very necessary in reuse and protection of high-value and fragile components.³⁰ For example, the out-of-plane adhesive strength of ChNCs (0.46 MPa) is nearly 6 times higher than that of cellulose nanocrystal adhesive (0.08 MPa). The inherent properties of ChNCs such as high strength (longitudinal modulus >150 GPa), high thermal stability (decomposition >240 °C), and high biocompatibility have widened the range of application of this novel green natural nanoglue.³¹

The adhesion stability is a critical factor for their practical application. From above, we know that ChNC nanoglue has high in-plane strength and low out-of-plane strength. Therefore, the in-plane stability was tested by a side knock test (Figure 2I). The sample remained bonded after several side knocks, and the glass sheets were still held together by the adhesive, which showed the good in-plane stability of ChNC nanoglue (Movie S3). Compared with the high in-plane strength, the out-of-plane strength of the adhesive is relatively weak. However, it is surprising that the adhesion of the sample did not fail after several front knocks and passed the out-of-plane stability test (Movie S4). Finally, the whole stability of the sample was examined by a dropping test. The sample was placed in the air at a height of 20 cm from the desktop and impacted the desktop several times freely (Movie S5). ChNC nanoglue exhibits excellent stability while maintaining high adhesion anisotropy, which can be attributed to the high contact area, strong hydrogen bonding, and van der Waals force interactions. Compared with cellulose nanoglue, the surprising stability of ChNCs indicates that this adhesive has greater application potential.¹²

Adhesion Mechanism of ChNC Nanoglue. According to previous studies, it was found that the ChNC suspension would self-assemble into a lamellar structure at high concentration.^{32,33} Polarized optical microscope (POM) images of ChNCs show that the rod-like ChNCs have good stability and show self-assembly behavior to form liquid crystal phase (Figure S1B). When the concentration of ChNCs was below 2 wt %, birefringence was not observed because of the isotropic phase of ChNCs. While for 4 wt % ChNC suspension, it was observed that the partially isotropic suspension transforms into an anisotropic crystalline liquid. Therefore, isotropic and liquid crystalline phases co-exist at this concentration. With the increase of the ChNC content, the liquid crystal phase ratio also increases. The fingerprint texture and birefringence were clearly observed in 8 wt % ChNC suspensions due to the parallel-alignment self-assembly of the nanocrystals (chiral nematic order).

The formation and long-range ordering of the superstructure occur during evaporation-induced self-assembly, which is a process of decreasing the water content and increasing the ChNC content. The increase of the ChNC content promotes the parallel alignment self-assembly of nanocrystals. It can be seen from Figure 3A that ChNCs were uniformly dispersed in water at the beginning. Gradually, the water evaporates led to the liquid film moving back, and the liquid crystal phase began to appear. Then, the liquid film broke down and formed a stripe. Finally, the stripe-shaped liquid film shrank into a long-range ordered superstructure stripe composed of stacked ChNCs. The gradual transformation of liquid film (pink) into a stripe (yellow) is the process of directional and ordered arrangement of ChNCs.

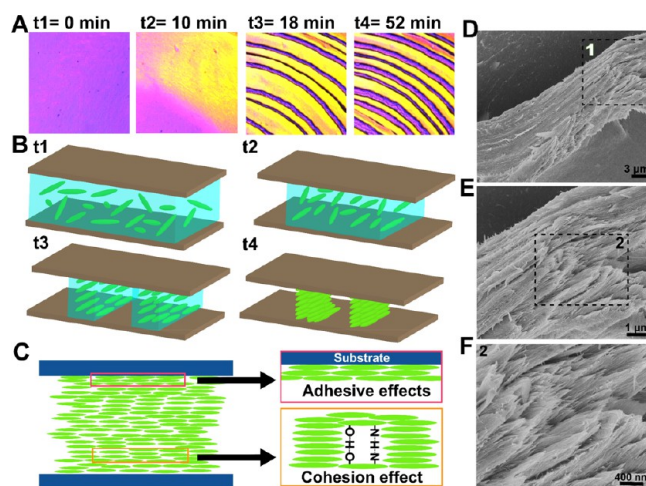


Figure 3. Adhesion mechanism of ChNC nanoglue. (A) POM images at different times in a corner of the ChNC bonding area. (B) Schematic illustration of the assembly mechanism highlighting steps t1–t4. (C) Illustration of the adhesion mechanism of the ChNC nanoglue. (D) SEM image of lamellae fractures of the ChNC superstructure. Magnified images of area 1 in (D) and area 2 in (E) highlighting the aligned ChNCs (F).

Precisely, the evaporation-induced self-assembly process can be divided into four different stages, t1–t4 (Figure 3B). At the t1 stage, ChNCs are uniformly distributed in the suspension, showing an isotropic phase (Movie S6). At the t2 stage, the liquid film begins to contract to the center of the overlapping area due to the evaporation of water. The content of ChNCs in the front of the liquid film increases, which promotes the orientation of ChNCs and the formation of the liquid crystal phase. At the t3 stage, the ChNC concentration reaches the critical threshold, the internal stress of the ChNC plane exceeds the tractive force of the gel suspension. Then, the branching initiation and propagation will occur. The first formed wide stripe splits into two strips, and the nanocrystals are further orientally aligned. At the t4 stage, free water evaporates completely. ChNC stripes are solidified by the supramolecular interaction that brings high internal cohesion and adhesion to the two surfaces via van der Waals (vdW) forces, capillary adhesion, and hydrogen bonding among the ChNCs and between ChNCs and substrates (Figure 3C).¹⁵

Here, the multilayer-oriented self-assembly structure of nanocrystals is similar to the bonding mode of polymer adhesives that possess flexible and interlocking molecular chains. When an adhesive layer was formed on the substrates, ChNCs arranged into a nematic phase would be in the maximum contact because of the affinity between the hydrogen bonds (O–H, N–H) on the surface and the anisotropy of ChNCs. The orientation of ChNCs in each stripe follows its main axis consistently, which can be seen from the fracture location in these structures (Figure 3D–F). The structured network of ChNCs brings extremely high cohesion and produces a huge spatial position lock to prevent its slippage. When the capillary force overcomes the water–ChNC interaction, ChNCs form high-strength supramolecular bonds.^{34,35} Van der Waals forces, hydrogen bonds, and coulomb interactions may be significantly affect these capillary forces and supramolecular bonds.³⁶ The sum of these interactions greatly enhances the adhesion among ChNCs. Therefore, multilayer assemblies of the ChNC

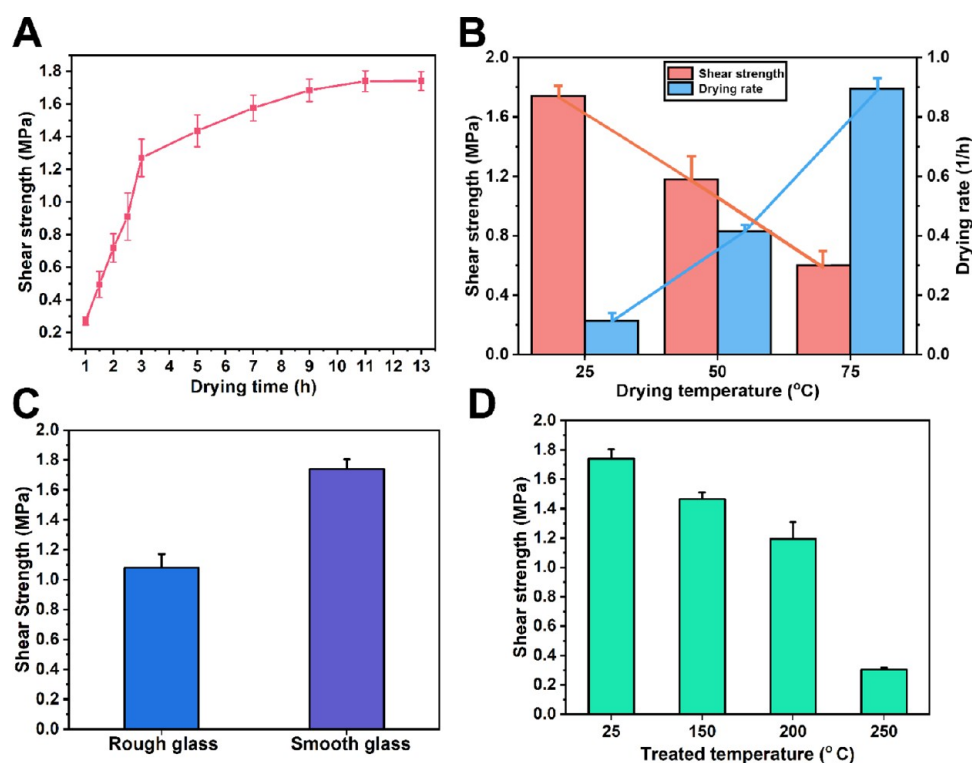


Figure 4. Effect of different factors on shear strength. (A) Drying time. (B) Drying temperature. (C) Substrate roughness. (D) Treated temperature.

contacting with the substrate results in the adhesion effect between the substrates.

Since the adhesion effect of ChNCs is formed by the water evaporation-induced self-assembly process, it can be inferred that the drying time has a significant effect on the adhesion strength. As shown in Figure 4A, the shear strength of ChNCs became stronger with the drying time increasing. At the beginning, the shear strength increased rapidly from 0.27 ± 0.03 MPa (1 h) to 1.27 ± 0.11 MPa (3 h). Then, the shear strength increased slowly from 1.27 ± 0.11 MPa (3 h) to 1.74 ± 0.06 MPa (11 h). Finally, the strength reached and stabilized at the maximum value of 1.74 ± 0.06 MPa. The increasing rate of shear strength in the early stage is faster than that in the later stage because the ChNC stripes are formed from the outside and the area (also the perimeter) of the stripe on the outer edge is larger than that on the inner region. In addition, the evaporation process is from the edge to the inside and the formed stripe will slow down the evaporation rate, which makes the evaporation rate of the edge faster than that of the inside.

Compared with the quick-drying adhesives (bonding time in a few seconds), the assembly time (1–11 h) of ChNC adhesives is relatively longer, but it is shorter than that of the common structural adhesives with curing time greater than 24 h.¹² Raising temperature is an effective way to speed up evaporation. It can be seen that the higher the drying temperature, the faster the drying rate (Figure 4B). However, the shear strength decreases with the increase of the drying rate because rapid drying reduces the long-range ordering of the microstructure. This suggests that the adhesive strength (1.74–0.60 MPa) and drying time (11.00–0.59 h) of the ChNC nanoglue can be adjusted by changing the drying temperature.

Roughness of the substrates always has a significant effect on the adhesion effect. Different from the rubber adhesives, the adhesion ability of ChNC nanoglue on rough glass is significantly lower than that of smooth glass, and the shear

strength decreases from 1.74 ± 0.06 to 1.08 ± 0.09 MPa (Figure 4C). Because the high shear strength of ChNCs is derived from the long-range ordered microstructure. Although the surface area of rough glass is larger than that of smooth glass, the uneven surface reduced the self-assembly efficiency of ChNCs. In contrast, the rubber adhesive shows increased adhesive strength on the rough surface since the polymer adhesion mechanism is related to the molecular chain entanglement.

As a high-performance adhesive, it is necessary to maintain high adhesive strength at high temperature treatment. The ChNC-glued glass samples were treated at high temperature for 24 h. It is found that the shear strength gradually decreases from 1.74 ± 0.06 (25 °C) to 1.46 ± 0.05 (150 °C), 1.19 ± 0.11 (200 °C), and 0.30 ± 0.01 MPa (250 °C). The shear strength at 200 °C is 68% to that at 25 °C (Figure 4D). The sharp decrease in adhesive strength at 250 °C is due to the decomposition of ChNCs at 245 °C (Figure 1G). Compared with the commercial 502 α -cyanoacrylate adhesive, which had lower temperature resistance (significant deterioration when the temperature higher than 100 °C), ChNC nanoglue has a wide application temperature range from 25 to 200 °C.

Failure Mechanism of ChNC Nanoglue. There are three main failure phenomena for adhesive-glued substrates: failure of adhesives themselves, debonding between adhesives and substrates, and failure of substrates. The changes before and after bonding failures were observed through a stereomicroscope (Figure 5A). Before the bonding failure, the complete ChNC stripes were fixed on the substrate in a long-range order. Most of the stripes were turned around on the corner of the glass sheet, which shows that the stripes are formed by the shrinkage of the ChNC liquid film along the contour of the substrate. The POM images taken at the corners also proved the long-range order of the stripes (Figure S4). Due to the birefringence of crystalline ChNCs, anisotropic aligned ChNCs would be observed in different interference colors (yellow and blue)

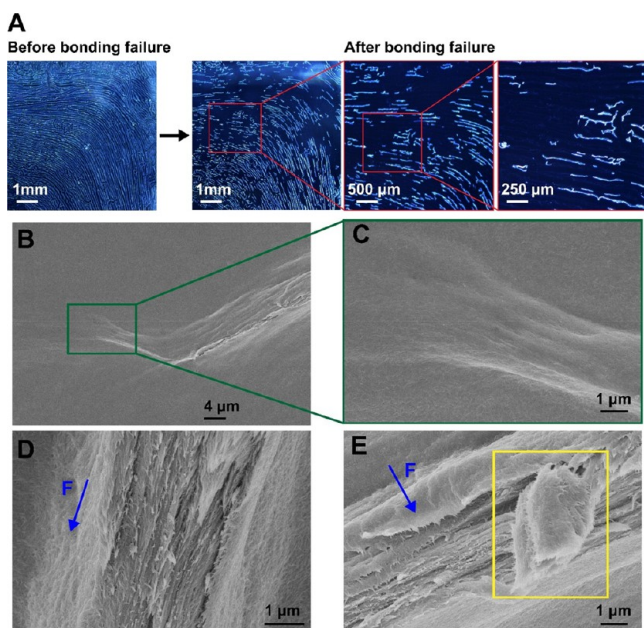


Figure 5. Failure mechanism of ChNC nanoglue. (A) Stereomicroscope pictures before and after bonding failures of the glass sheets. (B, C) Represented SEM images of adhesion failure between ChNC stripe and substrate. (D, E) The location of the bonding failure illustrating fracture of the stripe along the applied stress (blue arrows and “F” indicate the direction of the stresses, while the yellow box represents the semidetached ChNC stripe under stress).

under polarized light, while the isotropic region (substrates or disordered ChNC suspensions) would appear pink. The appearance of yellow and blue stripes confirmed the directional arrangement of ChNCs in the stripes observed in the SEM images above. After bonding failure, a small part of the stripes debonded from the structure, leaving a black structure part on the picture. In addition to the long-range ordered structure that grows along the edge, the ChNC adhesive also forms a worm-like structure in the inner section (Figure S2B). Although the contribution of the worm-like structure to the in-plane adhesive strength is lower than that of the linear structure, it certainly increased the bonding area, which improves the out-of-plane adhesive strength of ChNC adhesive.

Observing the junction between the white stripes and black substrate through SEM more microscopically, it can be seen that the stripes are indeed completely separated from the substrate under stress (Figure 5B,C). Most of the stripes left on the substrate had varying degrees of damage and lost their integrity during the debonding process (Figure 5D,E). The broken stripes were peeled off from the complete stripes, which indicates that the ChNC nanoglue itself had failed. When the stress was applied along the stripe direction, the orientation of ChNCs did not change significantly (Figure 5D). The orientation of ChNCs turned to the direction of the stress when the shear stress was applied perpendicular to the fringe direction (Figure 5E). The partial stripes (yellow boxes) that were in a semidetached state under stress further illustrate that the nematic ordered microstructure composed of ChNCs would debond itself under shear stress. From these results, it is clear that there are two main failure mechanisms of ChNC nanoglue as follows: the failure of the adhesive itself (mainly) and the debonding of the adhesive from the substrate (secondary).

It should be pointed out that the adhesion performance of the nanoglue comes from the unique shape and morphology of ChNCs. It was reported that the adhesion effect was attributed to the low-dimension anisotropic shape of nanoparticles. For example, the anisotropic coordination polymer nanocrystals show robust adhesion ability due to the stacking of nanoplates to form a lamellar structure, while the colloids with other morphologies such as cubes or nanospheres could not bind.¹⁵

Application of ChNC Nanoglue on Different Substrates. The versatility of the binding ability of ChNC nanoglue was investigated through various kinds of substrates. Figure 6A shows that ChNCs can bond a variety of materials, such as glass, metal, wood, polymers, and any combination therein. It is worth noting that no matter whether the surface of the substrate is flat (glass) or rough (wood), significant adhesive strength can still be realized. These results suggest that the bonding performance is not limited to specific surfaces, which makes ChNC nanoglue promising application in various areas. For example, wood can be well bonded by ChNC nanoglue, which illustrates that the green and nontoxic ChNC nanoglue has the potential to replace the chemical adhesives with high-volatile organic compounds contents. It may be used as a new generation of furniture adhesives.

ChNC nanoglue exhibits different binding capabilities on different substrates (Figure 6B). From the highest 1.74 ± 0.06 MPa (glass–glass) to the lowest 0.14 ± 0.02 MPa (wood–alumina), the difference in binding strengths on different substrates exceeds 10 times. We consider that the chemical properties of the substrate surface, especially hydrophilicity, affect the adhesion. Figure 6C shows that the water contact angle (CA) data of different substrates. The water contact angles of glass, wood, PMMA, steel, and alumina are $10.1 \pm 2.5^\circ$ (super hydrophilic), $23.5 \pm 4.0^\circ$ (quite hydrophilic), $72.4 \pm 2.7^\circ$ (weak hydrophilic), $110.1 \pm 2.9^\circ$ (quite hydrophobic), and $111.8 \pm 3.2^\circ$ (quite hydrophobic), respectively.

Comparing Figure 6B,C, it can be seen that the binding strength and hydrophilicity have a clear positive correlation. For example, the adhesion strength of wood–alumina (0.14 ± 0.02 MPa) is similar to that of wood–steel (0.16 ± 0.01 MPa) and both of them at low values, while the strength of wood–glass (0.84 ± 0.09 MPa) is much greater than them. The reason why the water contact angle causes such a large difference in adhesion strength is that ChNC suspension can fully wet the surfaces with high hydrophilicity. This further results in increased attractive capillary forces between surfaces.¹² Furthermore, the inherent interaction (such as hydrogen bonds) between the substrate and ChNCs may significantly increase the adhesion strength, for example, the cellulose (wood) and ChNCs.¹⁸ Therefore, the adhesion strength of ChNC nanoglue can be adjusted by choosing different substrates or modification of the substrates.

In view of the adhesive strength test, samples of different substrates showed different adhesive failure ways (Figure 6D). Cohesion failure means that the adhesive fails and the substrate itself remains intact. It occurs when the adhesion strength is lower than the material strength. Most of the tested samples showed cohesion failure. First, the PMMA, alumina, steel, and wood used as the substrate are sheets with a certain thickness, which have high strengths and are not easily broken. Second, ChNC nanoglue shows different adhesion strengths on different substrates. For example, the binding strength of ChNC nanoglue on the wood–steel substrate was only 0.16 ± 0.01 MPa and the cohesion failure occurred at a low load of 80.41 ± 1.72 N while the substrates still keep their integrity. Material failure means

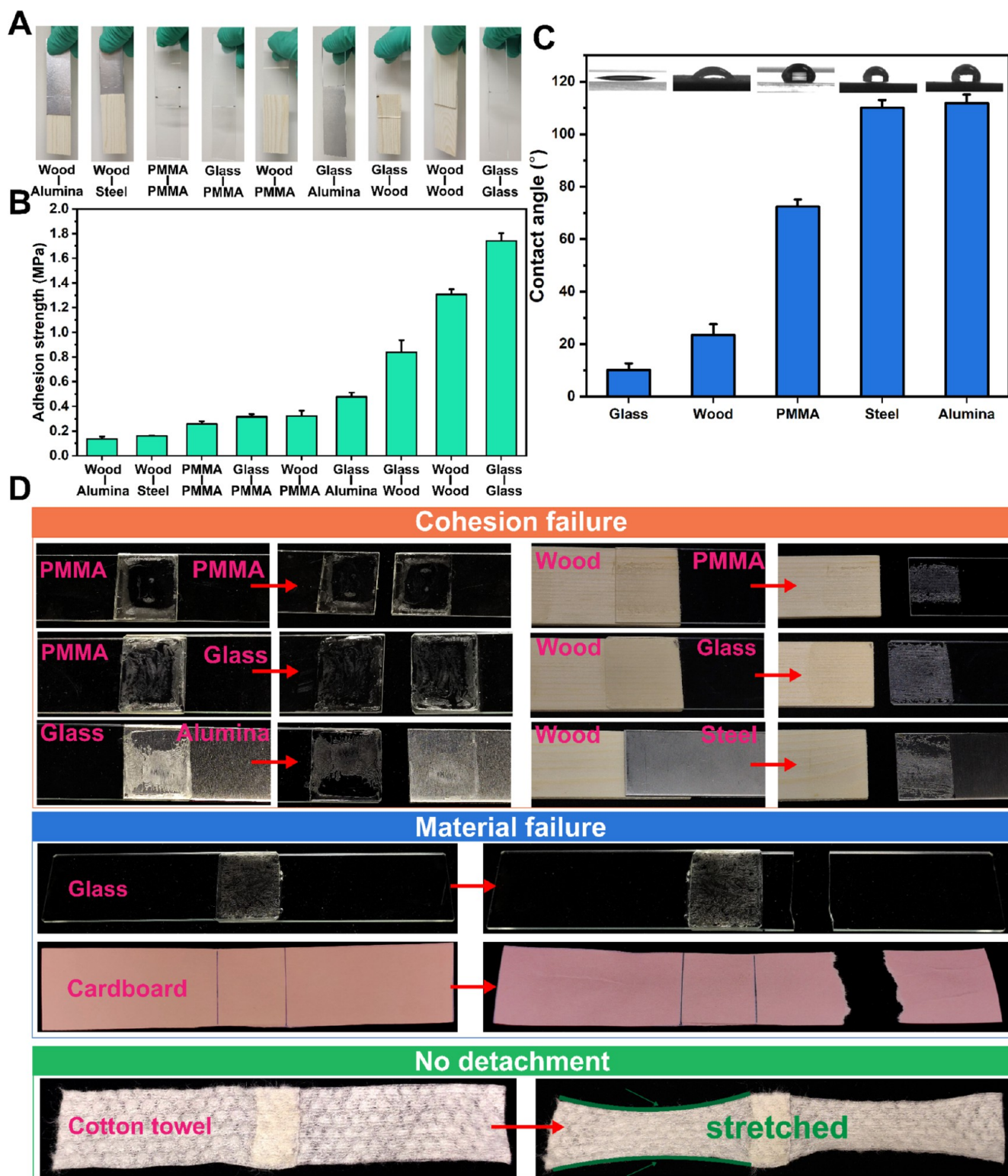


Figure 6. Application of ChNC nanoglu on different substrates. (A) Photos of various substrates bonded by ChNC nanoglu. (B) Shear adhesion strength of versatile surfaces glued by ChNC nanoglu (in all the cases, the loading densities of the powders are 0.8 mg cm^{-2}). (C) Water contact angle images and histogram of different substrates. (D) Photos of various substrates bonded with ChNC nanoglu before and after failure: the cohesion failures (orange box), the material failures (blue box), and no detachment of ChNCs rather showing material stretches (green box).

that the adhesive remains effective when the substrate breaks. This indicates the strong adhesion between the adhesive and substrate. A typical example is that, when the cardboards were broken by a pulling force of more than 200.00 N, the position bonded with ChNCs is still fixed. This shows that ChNC

nanoglu is very suitable for cardboard adhesive for children's manual work because of its high adhesive strength, nontoxicity, and short adhesive time (10 min). Two pieces of a cotton towel can be glued well, and the adhesion was still effective when cotton towels were deformed.³⁷

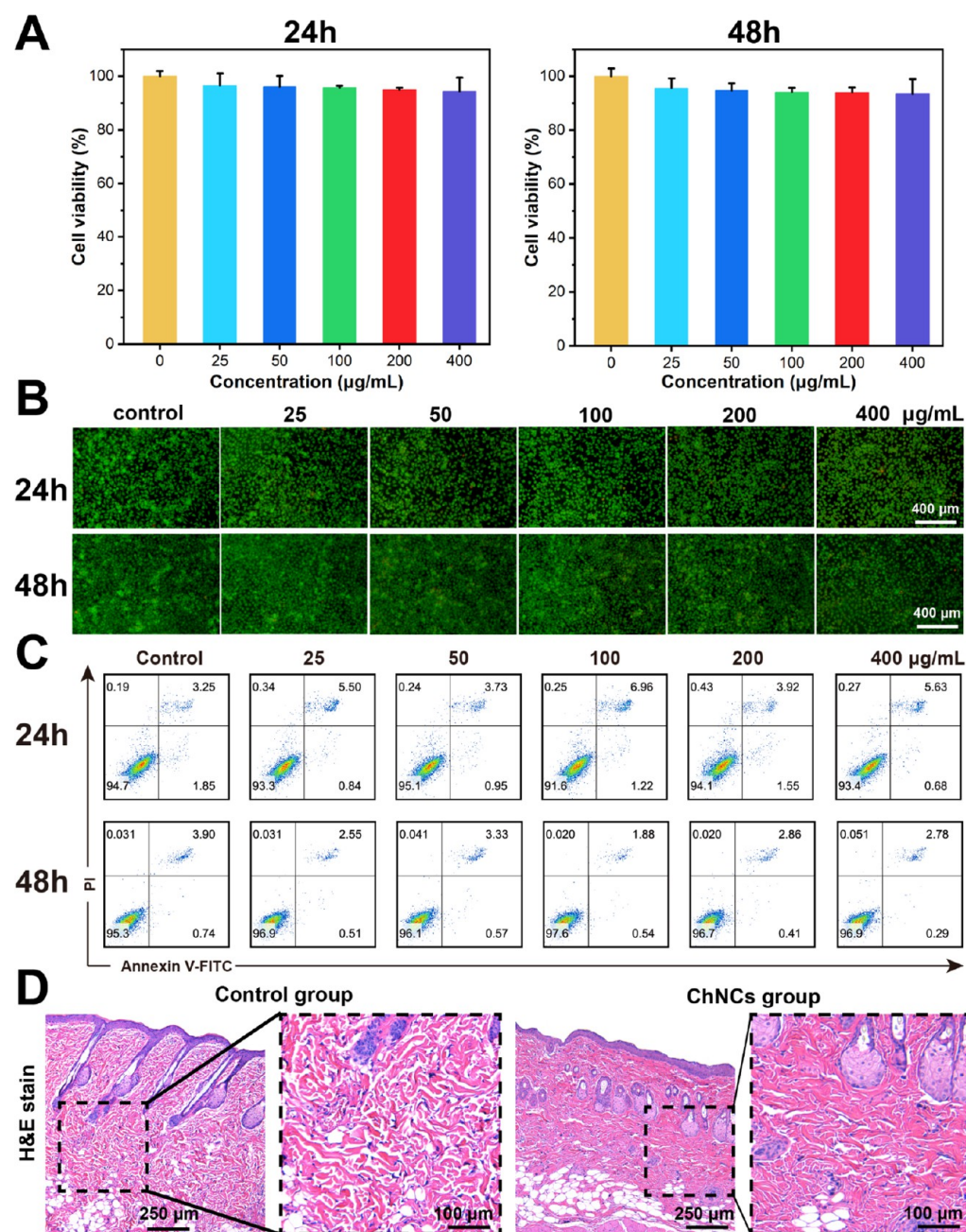


Figure 7. Biocompatibility of ChNC nanoglu. (A) Cytotoxicity of ChNC in vitro by the CCK-8 method. (B) AO/EB live/dead staining images of mouse fibroblasts (L-929) cultured for 24 and 48 h. (C) Apoptosis and necrosis results of L-929 cultured with ChNCs for 24 and 48 h (means \pm SD, $n = 3$) by the flow cytometry method. (D) H&E staining images of control skin and ChNC nanoglu-treated skin.

Paperboards were cut into different shapes to study the influence of the shape on the adhesion of the ChNC nanoglu (Table S1). The different shapes of the cardboard bonded with the ChNCs always are broken themselves during the tensile test, rather than the failure of the bonding position. These suggest that ChNC nanoglu is suitable for various substrates of different shapes.

Washability is an advantage of ChNC nanoglu over other commercial organic adhesives. A compared example was two pieces of glass sheets, which were bonded with double-sided tape. The residue after double-sided tape adhesive failure was hardly to be removed by washing. In contrast, the ChNC nanoglu is easily cleaned up by water washing and simply kneading because ChNCs have good water dispersibility (Figure

S5). The good washability demonstrates that the ChNC nanoglu is suitable for items that need to be reused. However, the water resistant is not good because ChNC nanoglu is a water-based adhesive. The water will destroy the hydrogen bond among the ChNCs and reduce the adhesion greatly. The water resistant may be improved by designing two-component nanoglu and introducing a covalent cross-linking bond.

Biocompatibility. As a promising daily-used adhesive, in vitro and in vivo biological safeties of ChNC nanoglu are critical in case of inevitable skin exposure. According to the previous researches on skin safety, we choose the mouse fibroblast cell line L929 as an in vitro model.^{38,39} The cytotoxicity of ChNCs was assessed by exposing L929 mouse fibroblasts to control and gradient concentrations of ChNCs for

24 h or 48 h. After treatment, we performed cell counting kit-8 (CCK-8) assay to investigate the cell viability. As shown in Figure 7A, the cell viabilities of the ChNC-treated groups are more than 95%, and it has no significant difference from the control groups, which reflects virtually no cytotoxicity of ChNCs.

To further visualize cell survival, the dual acridine orange/ethidium bromide (AO/EB) staining was used to distinguish live/dead cells. AO could penetrate in normal and early-apoptotic cells with intact membranes, appeared green fluorescence after binding with DNA. Meanwhile, EB would stain late-apoptotic and necrotic cells whose membranes were dented, fluorescing orange-red when binding to nuclear DNA. Figure 7B suggests that ChNC-treated groups maintain a large area of green and merely negligible orange-red fluorescence within the highest concentration of 400 $\mu\text{g}/\text{mL}$ at 24 or 48 h.

Subsequently, flow cytometry, a quantitative real-time cell detection method, was used to observe the population proportions of cells in different life cycles (Figure 7C). Annexin V-FITC negative/PI negative cells in the lower left quadrant are normal cells, and the remaining three quadrants represent early, mid-stage apoptotic, and necrotic cells, respectively. The Arabic numerals at the upper right of each quadrant are the proportions of the corresponding cell population. It is apparent that ChNC groups remain above 90% normal cells regardless of the concentrations and are no significant differences from the control. About 5% of spontaneous apoptotic cells is considered as normal because of the inevitably cell state fluctuations and the stimulation caused by sample preparation. In short, the results of the flow cytometry assays also confirm the excellent cytocompatibility of ChNC in vitro.

Our material is aimed to be used as industrial and household adhesives; therefore, the short-term skin contact evaluation was performed.^{40–42} We brushed ChNC suspension on the back skin of the pre-dehaired rats for 24 h ($n = 4$), visually inspected and sampled for histopathological analysis. No significant differences could be identified between the ChNC-contacted areas and untreated areas (control), both skin areas are normal without erythema, itching, or crack. In addition, the hematoxylin–eosin (H&E) staining results of skin cryosections also demonstrate that there are no obvious inflammatory cell infiltration (Figure 7D). Based on the in vitro results and skin safety test, ChNC nanogluue shows satisfied safety for skin contact.

CONCLUSIONS

The ChNC suspension can achieve a high-adhesive shear strength (about 5 MPa) by a simple self-assembly process via water evaporation. The assembly process leads to the transformation of the colloid from the liquid crystalline phase to the long-range ordered lamellar superstructure. The adhesion mode of the ChNC nanogluue-assembled superstructure is similar to that of polymer adhesive, and the adhesion and cohesion effect are related to the van der Waals force, capillary force, and hydrogen bond. Interestingly, the orientation of ChNCs results in a 10-fold difference in the in-plane and out-of-plane adhesion values. This anisotropic adhesion strength usually exists in gecko soles and insects, which were natural reversible adhesives. The high adhesion anisotropy does not cause the loss of stability. The knock and drop tests show that ChNC nanogluue-bonded samples have good shock stability. In addition, the adhesion ability of ChNC nanogluue is versatile to a variety of substrates such as glass, wood, metal, plastic, paper, and so on. As a water-

based adhesive, ChNC nanogluue has shown excellent biocompatibilities in cell and animal tests. In total, this study developed a green, eco-friendly, and water-based ChNC nanogluue with low cost, which has potential for adhesion in industrial and household applications.

MATERIALS AND METHODS

Materials. Crab shells were supplied by Wuhan Hezhong Biochemical Manufacturing Co., Ltd., China. Hydrochloric acid (HCl, 37%) was obtained from Guangzhou Chemical Reagent Factory. Smooth and frosted glass slides ($75 \times 25 \times 1$ mm) were purchased from Citotest Scientific Co., Ltd., China. PMMA, wood, alumina, steel, cardboard, cotton towel sheet, and sandpaper were purchased locally. The acridine orange/ethidium bromide (AO/EB) staining reagent was purchased from Beijing Solarbio Science & Technology Co., Ltd., China. The CCK-8 reagent was supplied from BestBio Biology Co., Ltd., China. Ultrapure water was purified by deionization and filtration with a Millipore purification apparatus (resistivity >18.2 M Ω .cm). Other chemicals of analytical grades were purchased from Aladdin Industrial Corp., China.

Preparation of the Chitin Nanocrystal (ChNC) Powder. According to a previous study,⁴³ ChNC powder was prepared by acid hydrolysis. Twenty grams of clean crab shells and 1 L HCl (3 mol/L) were added to a three-necked flask with oil bath heating and stirring at 104 °C for 3 h. The mixture was washed by centrifugation with ultrapure water at 6000 rpm for 5 min after acid hydrolysis. This process was repeated several times to remove excess acid and the amorphous phase. Then, the suspension was dialyzed in running water until the pH value of the suspension was close to 7.0. Finally, the suspension was frozen and the ChNC powder was collected by 24 h freeze-drying in a SCIENTZ-12ND vacuum freeze-dryer (Ningbo Scientz Biotechnology Co., Ltd., China).

Preparation of ChNC Suspension. Different ChNC suspensions were prepared using an ultrasonic treatment method. In a typical procedure, 1, 2, 4, and 8 wt % ChNC suspensions were obtained uniformly by dispersing ChNCs in ultrapure water via an ultrasonic cell disruptor (XM-1800T, ShangHai JingXin Industrial Development Co., Ltd., China) at 1500 W for 30 min.

Gluing of the Glass Sheet Samples. A drop of 25 μL of ChNC suspension was dropped on the glass substrate (length \times width \times thickness: $60\text{--}75 \times 25 \times 1\text{--}2$ mm). To keep force balance and uniform contacting, another glass sheet with the same thickness was placed under the top glass sheet. The overlap area was between 1 and 2×2.5 cm (length \times width). The samples were dried in a fume hood for at least 3 h at ca. 70% relative humidity and 25 °C. Some samples were dried in air circulation oven at 50–250 °C for different times to study the relationship between the temperature and drying time.

Gluing of Other Substrates Samples. Carboard, steel sheet, alumina sheet, and wood samples were all glued using the standard protocol similar to the glass sheet. Samples were also glued by drying a drop of ChNC suspension on each substrate. To change the geometry of the substrates, cardboards were cut into different shapes and aspect ratios prior to gluing.

Cell Culture. As biosafety assessment model system, the mouse fibroblast (L929) cell line from American Type Culture Collection (ATCC) was used. It was maintained in the minimum essential medium (MEM) (C12571500BT, Life Technologies, USA) supplemented with 10% fetal bovine serum (10270-106, Gibco, USA) and 1% penicillin–streptomycin (15140122, Gibco, USA). The cell line and treated plates were cultured at 37 °C in a 5% CO₂ and 95% air-humidified incubator.

Characterization of the ChNC Suspension. A ChNC suspension of 0.05 wt % was prepared for TEM, AFM, particle size distribution, and ζ -potential testing. The morphology of ChNCs was analyzed by transmission electron microscopy (TEM; JEM, 1400 Flash) and atomic force microscopy (AFM; Bioscope Catalyst Nano scope-V, Bruker Instruments Ltd., USA). The particle size distribution and ζ potential of the ChNC dispersion were obtained using a Nano ZS ζ -potential analyzer (Malvern Instruments Co., U.K.). FTIR spectra of ChNCs

obtained with Thermo FTIR (Nicolet iS50, Thermo Fisher Scientific Co. Ltd., USA) and the X-ray diffraction (XRD) patterns were recorded using a Miniflex600, Rigaku Corp, Japan, Cu-K α radiation. The thermogravimetric analysis (TGA) was conducted using a TGA machine (TGA2, METTLER TOLEDO Co. Ltd., Switzerland). ChNC suspensions were observed with a polarized optical microscope (POM; BX51, Olympus, Japan).

Morphology and Structure of ChNC Nanoglue. Polarized microscopy (POM) images and videos were obtained using the ChNC suspension sample above, and self-assembly process was recorded by adding a 530 nm compensating plate on a POM machine at a fixed working distance. Dark-field imaging images were taken by a stereomicroscope (ZEISS SteREO Discovery V 20) to obtain the sharp contrast and large imaging area. The geometric morphology of ChNC nanoglue structure was observed by an FE-SEM (ULTRASS, Carl Zeiss Jena Co. Ltd., Germany) at 5 kV. Before FE-SEM observation, the samples were sputter-coated with gold films with a thickness of 5 nm.

Calculation of Contact Area. Dark-field imaging images were taken by the stereomicroscope (ZEISS SteREO Discovery V 20) to obtain the sharp contrast and large imaging area. The contact area was estimated by thresholding and filtering for bright areas within the overlap area of the bond using ImageJ software from pictures taken by the stereomicroscope.

Lap-Shear and Out-of-Plane Adhesion Tests of ChNC Nanoglue. To measure the lap-shear strength, a universal testing machine (Z005, Zwick/Roell Co. Ltd., Germany) was used. The distance between fixtures was 40 mm, and the strain rate was 1.5 mm·min⁻¹. The overlap length was kept as 10 or 20 mm. Because of the high bond anisotropy, the samples were clamped between sandpapers to minimize out-of-plane stresses (Figure S6A). Five-to-ten samples were evaluated, and the standard deviation and average were provided for each group. The samples were kept at 70% relative humidity prior to the measurement. The maximum load before catastrophic failure was used to calculate the adhesion strength. Out-of-plane tests were measured by the three-point bending test. The distance between fixtures was 40 mm. The sample was placed in the middle of the fixture and a shim of the same thickness was added to balance the pressure on both sides (Figure S6B). Cardboard samples broke before the adhesive broke, thereby preventing accurate measurements. Because of high anisotropy in adhesive strengths and high hardness of the substrates, the adhesive strength in-plane values of alumina and steel plates glued by ChNC nanoglue were not accurately measured.

Stability Test of ChNC Nanoglue. To examine in-plane and out-of-plane stabilities, the glass sheet samples (overlap length: 20 mm) were knocked on the desk several times from two different directions. The samples were dropped several times from a height of 20 cm to test the whole stability.

Washability Test. Two glass sheets were bonded together by ChNC nanoglue or commercial double-sided tape for 24 h, respectively. The samples were peeled off after bonding completely and washed by running water and kneading gently for 30 s. Finally, the samples were air dried and photographed.

Cytotoxicity and LIVE/DEAD Staining Assays. The cell counting kit 8 (CCK-8) assay was used for cytotoxicity evaluation. L929 cells (3×10^4 cells/mL) at the logarithmic growth phase were inoculated (100 μ L/well) in a 96-well plate (3599, Corning, USA). The plate was pre-incubated in a humidified incubator overnight for cell adherence. A Medium without cells for blank control was used. Cells were treated with ChNCs at the following concentration: 0, 25, 50, 100, 200, 400 μ g/mL. An amount of 0 μ g/mL was used as for control. After 24 or 48 h treatment, An amount of 10 μ L of CCK-8 solution was added into each well for additional 4 h. Afterward, the plate was gently mixed on an orbital shaker for 1 min to ensure homogeneous distribution of color. Next, the absorbance at 450 nm was measured using a microplate reader (Bio-Tek, Hercules, USA). Each experiment was performed three times. The percentages of cell viability were calculated by (OD value of the ChNC group - OD value of the blank control) / (OD value of the 0 μ g/mL control group - OD value of the blank control) \times 100%.

Morphological evidences of death/live cells were analyzed using acridine orange/ethidium bromide (AO/EB) staining. AO is permeable to both dead and live cells, whereas EB can penetrate into dead cells and combines with their DNA and RNA. Hence, the live cells will appear green and dead cells become yellow or orange. L929 cells were inoculated (3×10^4 cells/mL, 1 mL/well) in a 24-well plate (3524, Corning, USA) and treated with 0, 25, 50, 100, 200, 400 μ g/mL ChNCs. An amount of 0 μ g/mL was the control. After incubated at 37 $^{\circ}$ C in 5% CO₂ for 24 or 48 h, the culture supernatants were removed and washed twice with PBS (C10010500BT, Gibco, USA). AO (100 μ g/mL), EB (100 μ g/mL) and PBS buffer were mixed at a ratio of 1:1:100. Added 500 μ L staining solution each well and incubated for 10 min at room temperature without light. The staining solution was removed and used 100 μ L of PBS for madeaction. Cells were visualized under a fluorescence microscope (XDY-2, Guangzhou Liss Optical Instrument Ltd., China), and images were taken in random fields.

Flow Cytometry of Annexin V-FITC/PI Assay. Two milliliters of L929 cells (3×10^4 /mL) were inoculated into 6-well plates overnight for cell adherence and treated with 0, 25, 50, 100, 200, and 400 μ g/mL ChNCs. After cultured in an air-humidified incubator for 24 or 48 h, cells were washed with PBS and gently digested by EDTA-free trypsin (0.25%) (1505006S, Gibco, USA). Collected cells at 800 g for 5 min were centrifuged and suspended in 400 μ L of binding buffer. FITC-conjugated Annexin-V and propidium iodide (PI) (respectively, 5 μ L of each tube) were used to distinguish cells in different apoptosis cycles.⁴⁴ After incubated for 10 min at room temperature without light, 1×10^5 stained cells were analyzed using a BD FACSCanto II flow cytometer (BD Biosciences, USA). Fluorescence was detected with the following bandpass filters: 530 nm for Annexin-V-FITC and 670 nm for PI. The results were analyzed by the FlowJo 10.0.2 (BD Biosciences, USA).

In Vivo Skin Irritation. Male Sprague–Dawley (SD) rats ($n = 4$, 8–9 weeks old, 200–350 g) were obtained from Guangdong Pharmaceutical University Undergraduate Laboratory Animal Center (Guangzhou, China) and raised in Institute of Laboratory Animal of Jinan University (Guangzhou, China). Animals were fed ad libitum and performed in compliance with the National Ethics Committee on Animal Welfare of China. Rats were anesthetized with isoflurane (4% in 100% oxygen for induction, 2% for maintenance) on thermal pads in case of hypothermia. Rat back hairs were removed with an electric razor, and depilatory cream (Veet, France) was used to cleaned up residual hairs.⁴⁵ After disinfected with medicinal alcohol, ChNCs were applied to a specific area (15 mm by 15 mm) on the rat back (the untreated area was more than 10 mm from the ChNC location as normal skin control). To prevent ChNCs from being scratched off by rats, we used medical gauze (3M, USA) to protect the samples. After 24 h, the results were recorded whether there was erythema, itching, or crack in the testing areas, and ChNCs were cleaned up thoroughly. Skins (10 \times 10 mm) for histological analyses were sampled by surgical scissors and soaked in 4% paraformaldehyde solution for tissue fixation. Cryosections (6 μ m) of all samples were stained with hematoxylin–eosin (H&E) reagents and then microscopically observed.⁴⁶

■ ASSOCIATED CONTENT

Supporting Information

The Supporting Information is available free of charge at <https://pubs.acs.org/doi/10.1021/acsami.1c02000>.

Digital and POM images of different concentrations of ChNC aqueous suspensions, contact area of ChNC nanoglue, anisotropy of shear strength for different adhesives, POM image of ChNC adhesive layers and corresponding lamellae, photos of ChNC nanoglue and double-sided adhesive before and after washing, illustration of adhesion strength test methods, and table of adhesion failures of cardboards with different shapes (PDF)

In-plane load test of the glass sample (MP4)

Out-of-plane load test of the glass sample (MP4)

Side knock test of the glass sample (MP4)

Front knock test of the glass sample (MP4)
Drop test of the glass sample (MP4)
Formation of the bonding structure (MP4)

AUTHOR INFORMATION

Corresponding Author

Mingxian Liu – Department of Materials Science and Engineering, Jinan University, Guangzhou 510632, China;
orcid.org/0000-0002-5466-3024; Email: liumx@jnu.edu.cn

Authors

Hongzhong Liu – Department of Materials Science and Engineering, Jinan University, Guangzhou 510632, China
Yue Feng – Department of Materials Science and Engineering, Jinan University, Guangzhou 510632, China
Xiang Cao – Department of Materials Science and Engineering, Jinan University, Guangzhou 510632, China
Binghong Luo – Department of Materials Science and Engineering, Jinan University, Guangzhou 510632, China;
orcid.org/0000-0001-8689-4196

Complete contact information is available at:
<https://pubs.acs.org/10.1021/acsami.1c02000>

Author Contributions

Conception and design were performed by H.Z.L., Y.F., X.C., B.H.L., and M.X.L.; experiments were executed by H.Z.L., Y.F., and X.C.; analyses were done by H.Z.L. and Y.F.; writing was carried out by H.Z.L. and Y.F. with contributions from H.Z.L., Y.F., X.C., B.H.L., and M.X.L.; review and editing were executed by H.Z.L., Y.F., X.C., B.H.L., and M.X.L.; and supervision and funding acquisition were done by M.X.L.

Notes

The authors declare no competing financial interest.

ACKNOWLEDGMENTS

This work was financially supported by the National Natural Science Foundation of China (52073121), Natural Science Foundation of Guangdong Province (2019A1515011509), Science and Technology Planning Project of Guangdong Province (2019A050513004), and the Fundamental Research Funds for the Central Universities (21619102).

REFERENCES

- (1) Karnal, P.; Roberts, P.; Gryska, S.; King, C.; Barrios, C.; Frechette, J. Importance of Substrate Functionality on the Adhesion and Debonding of a Pressure-Sensitive Adhesive under Water. *ACS Appl. Mater. Interfaces* **2017**, *9*, 42344–42353.
- (2) Park, S.; Kim, M.; Kwak, D.; Im, G.; Park, J. J. Skinlike Disposable Tattoo on Elastic Rubber Adhesive with Silver Particles Penetrated Electrode for Multipurpose Applications. *ACS Appl. Mater. Interfaces* **2018**, *10*, 16932–16938.
- (3) Lührs, A. K.; De Munck, J.; Geurtsen, W.; Van Meerbeek, B. Composite Cements Benefit from Light-Curing. *Dent. Mater.* **2014**, *30*, 292–301.
- (4) Hong, X.; Wen, J.; Xiong, X.; Hu, Y. Silver Nanowire-Carbon Fiber Cloth Nanocomposites Synthesized by UV Curing Adhesive for Electrochemical Point-of-Use Water Disinfection. *Chemosphere* **2016**, *154*, 537–545.
- (5) Jeong, H. E.; Lee, J. K.; Kim, H. N.; Moon, S. H.; Suh, K. Y. A Nontransferring Dry Adhesive with Hierarchical Polymer Nanohairs. *Proc. Natl. Acad. Sci. U. S. A.* **2009**, *106*, 5639–5644.

- (6) Łebkowska, M.; Załęska-Radziwiłł, M.; Tabernacka, A. Adhesives Based on Formaldehyde – Environmental Problems. *BioTechnologia* **2017**, *98*, 53–65.
- (7) Nielsen, G. D.; Larsen, S. T.; Wolkoff, P. Re-Evaluation of The WHO (2010) Formaldehyde Indoor Air Quality Guideline for Cancer Risk Assessment. *Arch. Toxicol.* **2017**, *91*, 35–61.
- (8) Dunky, M. Urea-Formaldehyde (UF) Adhesive Resins for Wood. *Int. J. Adhes. Adhes.* **1998**, *18*, 95–107.
- (9) Hun, D. E.; Corsi, R. L.; Morandi, M. T.; Siegel, J. A. Formaldehyde in Residences: Long-Term Indoor Concentrations and Influencing Factors. *Indoor Air* **2010**, *20*, 196–203.
- (10) Liu, M.; He, R.; Yang, J.; Zhao, W.; Zhou, C. Stripe-like Clay Nanotubes Patterns in Glass Capillary Tubes for Capture of Tumor Cells. *ACS Appl. Mater. Interfaces* **2016**, *8*, 7709–7719.
- (11) He, R.; Liu, M.; Shen, Y.; Long, Z.; Zhou, C. Large-Area Assembly of Halloysite Nanotubes For Enhancing the Capture of Tumor Cells. *J. Mater. Chem. B* **2017**, *5*, 1712–1723.
- (12) Tardy, B. L.; Richardson, J. J.; Greca, L. G.; Guo, J.; Ejima, H.; Rojas, O. J. Exploiting Supramolecular Interactions from Polymeric Colloids for Strong Anisotropic Adhesion between Solid Surfaces. *Adv. Mater.* **2020**, *32*, 1906886.
- (13) Kryuchkova, M.; Batasheva, S.; Naumenko, E.; Rozhina, E.; Akhatova, F.; Panchal, A.; Lvov, Y.; Fakhrullin, R. Self-Assembly of Concentric Microrings of Tubule and Platy Nanoclays for Cell Patterning and Capturing. *Appl. Clay Sci.* **2020**, *195*, 105707.
- (14) Batasheva, S.; Kryuchkova, M.; Fakhrullin, R.; Cavallaro, G.; Lazzara, G.; Akhatova, F.; Nigamatzyanova, L.; Evtugyn, V.; Rozhina, E.; Fakhrullin, R. Facile Fabrication of Natural Polyelectrolyte-Nanoclay Composites: Halloysite Nanotubes, Nucleotides and DNA Study. *Molecules* **2020**, *25*, 3557.
- (15) Zhao, Y.; Li, W.; Jiang, X.; Li, F.; Li, X.; Zhang, W.; Jiang, J. S.; Liu, J.; Ariga, K.; Hu, M. Coordination Polymer Nanogluue: Robust Adhesion Based on Collective Lamellar Stacking of Nanoplates. *ACS Nano* **2017**, *11*, 3662–3670.
- (16) Cavallaro, G.; Micciulla, S.; Chiappisi, L.; Lazzara, G. Chitosan-Based Smart Hybrid Materials: a Physico-Chemical Perspective. *J. Mater. Chem. B* **2021**, *9*, 594–611.
- (17) Merzendorfer, H.; Zimoch, L. Chitin Metabolism in Insects: Structure, Function and Regulation of Chitin Synthases and Chitinases. *J. Exp. Biol.* **2003**, *206*, 4393–4412.
- (18) Salaberria, A. M.; Labidi, J.; Fernandes, S. C. M. Chitin Nanocrystals and Nanofibers as Nano-Sized Fillers into Thermoplastic Starch-Based Biocomposites Processed by Melt-Mixing. *Chem. Eng. J.* **2014**, *256*, 356–364.
- (19) Fan, Y.; Saito, T.; Isogai, A. Chitin Nanocrystals Prepared by TEMPO-Mediated Oxidation of α -Chitin. *Biomacromolecules* **2008**, *9*, 192–198.
- (20) Fan, Y.; Saito, T.; Isogai, A. Preparation of Chitin Nanofibers from Squid Pen β -chitin by Simple Mechanical Treatment under Acid Conditions. *Biomacromolecules* **2008**, *9*, 1919–1923.
- (21) Lu, Y.; Weng, L.; Zhang, L. Morphology and Properties of Soy Protein Isolate Thermoplastics Reinforced with Chitin Whiskers. *Biomacromolecules* **2004**, *5*, 1046–1051.
- (22) Gopalan Nair, K.; Dufresne, A.; Gandini, A.; Belgacem, M. N. Crab Shell Chitin Whiskers Reinforced Natural Rubber Nanocomposites. 3. Effect of Chemical Modification of Chitin Whiskers. *Biomacromolecules* **2003**, *4*, 1835–1842.
- (23) Zeng, J. B.; He, Y. S.; Li, S. L.; Wang, Y. Z. Chitin Whiskers: an Overview. *Biomacromolecules* **2012**, *13*, 1–11.
- (24) Kumar, M. R. Chitin and Chitosan Fibres: a Review. *Bull. Mater. Sci.* **1999**, *22*, 905.
- (25) Zhao, X.; Wan, Q.; Fu, X.; Meng, X.; Ou, X.; Zhong, R.; Zhou, Q.; Liu, M. Toxicity Evaluation of One-Dimensional Nanoparticles Using *Caenorhabditis Elegans*: A Comparative Study of Halloysite Nanotubes and Chitin Nanocrystals. *ACS Sustainable Chem. Eng.* **2019**, *7*, 18965–18975.
- (26) Revol, J. F.; Marchessault, R. H. In Vitro Chiral Nematic Ordering of Chitin Crystallites. *Int. J. Biol. Macromol.* **1993**, *15*, 329–335.

- (27) Ifuku, S.; Nogi, M.; Abe, K.; Yoshioka, M.; Morimoto, M.; Saimoto, H.; Yano, H. Preparation of Chitin Nanofibers with a Uniform Width as α -Chitin from Crab Shells. *Biomacromolecules* **2009**, *10*, 1584–1588.
- (28) Ou, X.; Zheng, J.; Zhao, X.; Liu, M. Chemically Cross-Linked Chitin Nanocrystal Scaffolds for Drug Delivery. *ACS Appl. Nano Mater.* **2018**, *1*, 6790–6799.
- (29) Kaaden, C.; Powers, J. M.; Friedl, K.-H.; Schmalz, G. Bond Strength of Self-Etching Adhesives to Dental Hard Tissues. *Clin. Oral Investig.* **2002**, *6*, 155–160.
- (30) Stahel, W. R. The Circular Economy. *Nature* **2016**, *531*, 435–438.
- (31) Huang, Y.; Yao, M.; Zheng, X.; Liang, X.; Su, X.; Zhang, Y.; Lu, A.; Zhang, L. Effects of Chitin Whiskers on Physical Properties and Osteoblast Culture of Alginate Based Nanocomposite Hydrogels. *Biomacromolecules* **2015**, *16*, 3499–3507.
- (32) Yamamoto, Y.; Nishimura, T.; Saito, T.; Kato, T. CaCO₃/Chitin-Whisker Hybrids: Formation of CaCO₃ Crystals in Chitin-Based Liquid-Crystalline Suspension. *Polym. J.* **2010**, *42*, 583–586.
- (33) Liu, W.; Liu, K.; Zhu, L.; Li, W.; Liu, K.; Wen, W.; Liu, M.; Li, H.; Zhou, C.; Luo, B. Liquid Crystalline and Rheological Properties of Chitin Whiskers with Different Chemical Structures and Chargeability. *Int. J. Biol. Macromol.* **2020**, *157*, 24–35.
- (34) Gardner, D. J.; Oporto, G. S.; Mills, R.; Samir, M. A. S. A. Adhesion and Surface Issues in Cellulose and Nanocellulose. *J. Adhes. Sci. Technol.* **2008**, *22*, 545–567.
- (35) Mittal, N.; Ansari, F.; Gowda, V. K.; Brouzet, C.; Chen, P.; Larsson, P. T.; Roth, S. V.; Lundell, F.; Wagberg, L.; Kotov, N. A.; Soderberg, L. D. Multiscale Control of Nanocellulose Assembly: Transferring Remarkable Nanoscale Fibril Mechanics to Macroscale Fibers. *ACS Nano* **2018**, *12*, 6378–6388.
- (36) Hirn, U.; Schennach, R. Comprehensive Analysis of Individual Pulp Fiber Bonds Quantifies the Mechanisms of Fiber Bonding in Paper. *Sci. Rep.* **2015**, *5*, 10503.
- (37) Hollister, S. J. Porous Scaffold Design for Tissue Engineering. *Nat. Mater.* **2005**, *4*, 518–524.
- (38) Leelanarathiwat, K.; Minato, K.; Katsuta, Y.; Otsuka, Y.; Katsuragi, H.; Watanabe, F. Cytotoxicity of Hydroxyapatite-Tyrosine Complex with Gray Titania Coating on Titanium Alloy Surface to L929 Mouse Fibroblasts. *Dent. Mater. J.* **2019**, *38*, 573–578.
- (39) Kanimozhi, K.; Basha, S. K.; Kaviyarasu, K.; SuganthaKumari, V. Salt Leaching Synthesis, Characterization and in Vitro Cytocompatibility of Chitosan/Poly (Vinyl Alcohol)/Methylcellulose–ZnO Nanocomposites Scaffolds Using L929 Fibroblast Cells. *J. Nanosci. Nanotechnol.* **2019**, *19*, 4447–4457.
- (40) Todo, H. Transdermal Permeation of Drugs in Various Animal Species. *Pharmaceutics* **2017**, *9*, 33.
- (41) Khalaf, A. A.; Hassanen, E. I.; Azouz, R. A.; Zaki, A. R.; Ibrahim, M. A.; Farroh, K. Y.; Galal, M. K. Ameliorative Effect Of Zinc Oxide Nanoparticles Against Dermal Toxicity Induced By Lead Oxide In Rats. *Int. J. Nanomed.* **2019**, *Volume 14*, 7729–7741.
- (42) Rao, R. S.; Medhi, B.; Saikia, U. N.; Arora, S. K.; Toor, J. S.; Khanduja, K. L.; Pandhi, P. Experimentally Induced Various Inflammatory Models and Seizure: Understanding the Role of Cytokine in Rat. *Eur. Neuropsychopharmacol.* **2008**, *18*, 760–767.
- (43) Wongpanit, P.; Sanchavanakit, N.; Pavasant, P.; Bunaprasert, T.; Tabata, Y.; Rujiravanit, R. Preparation and Characterization of Chitin Whisker-Reinforced Silk Fibroin Nanocomposite Sponges. *Eur. Polym. J.* **2007**, *43*, 4123–4135.
- (44) Brodoceanu, D.; Bauer, C. T.; Kroner, E.; Arzt, E.; Kraus, T. Hierarchical Bioinspired Adhesive Surfaces—a Review. *Bioinspir. Biomim.* **2016**, *11*, No. 051001.
- (45) Korat, P. S.; Kapupara, P. P. Local Infiltration of the Surgical Wound with Levobupivacaine, Ibuprofen, and Epinephrine in Post-operative Pain: An Experimental Study. *Biomed. Pharmacother.* **2017**, *96*, 104–111.
- (46) Assmann, A.; Delfs, C.; Munakata, H.; Schiffer, F.; Horstkötter, K.; Huynh, K.; Barth, M.; Stoldt, V. R.; Kamiya, H.; Boeken, U.; Lichtenberg, A.; Akhyari, P. Acceleration of Autologous in Vivo

Supporting information
Chitin Nanocrystals as an Eco-friendly and Strong Anisotropic
Adhesive

*Hongzhong Liu, Yue Feng, Xiang Cao, Binghong Luo, Mingxian Liu**

Department of Materials Science and Engineering, Jinan University, Guangzhou 510632,

China

*Corresponding author. Email: liumx@jnu.edu.cn

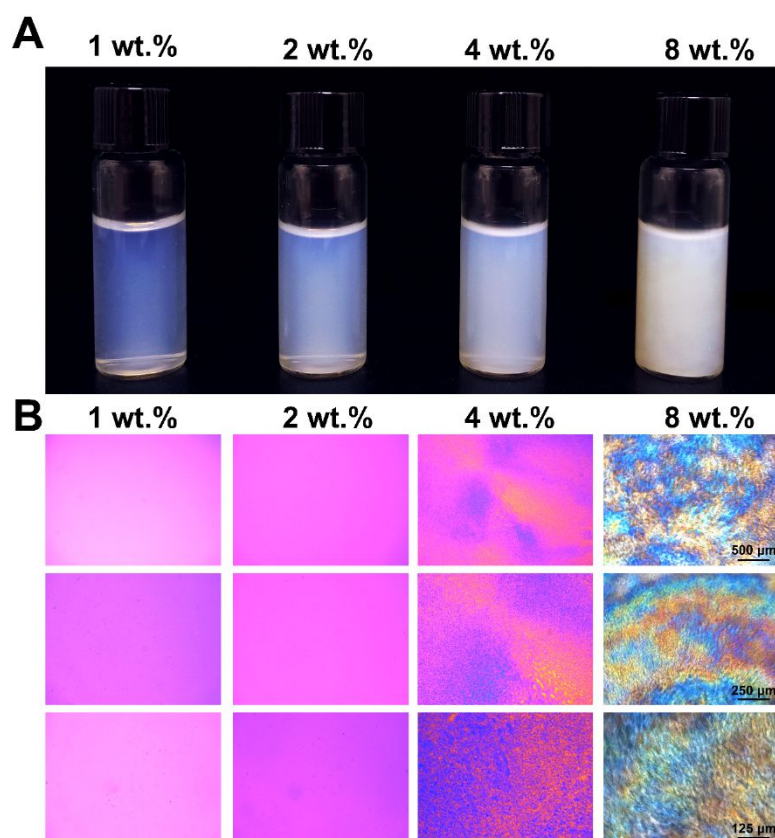


Figure S1. (A) Images of different concentrations of ChNCs aqueous suspensions. (B) Polarized optical microscopy images of different concentrations of ChNCs suspensions with different magnifications of 50X, 100X, and 200X.

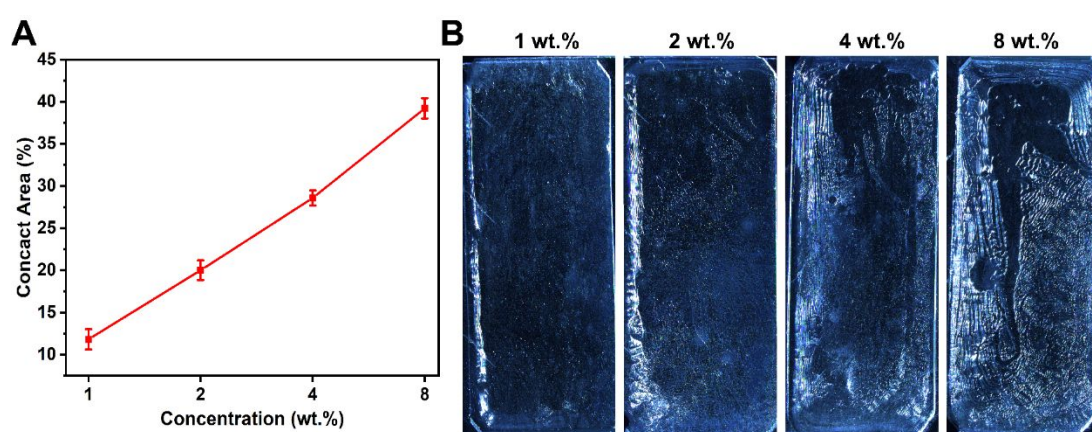


Figure S2. Contact area of ChNCs nanoglue. (A) Relationship between ChNCs suspension concentrations and contact area within the overlapping area. (B) 4 examples are shown at varying concentrations.

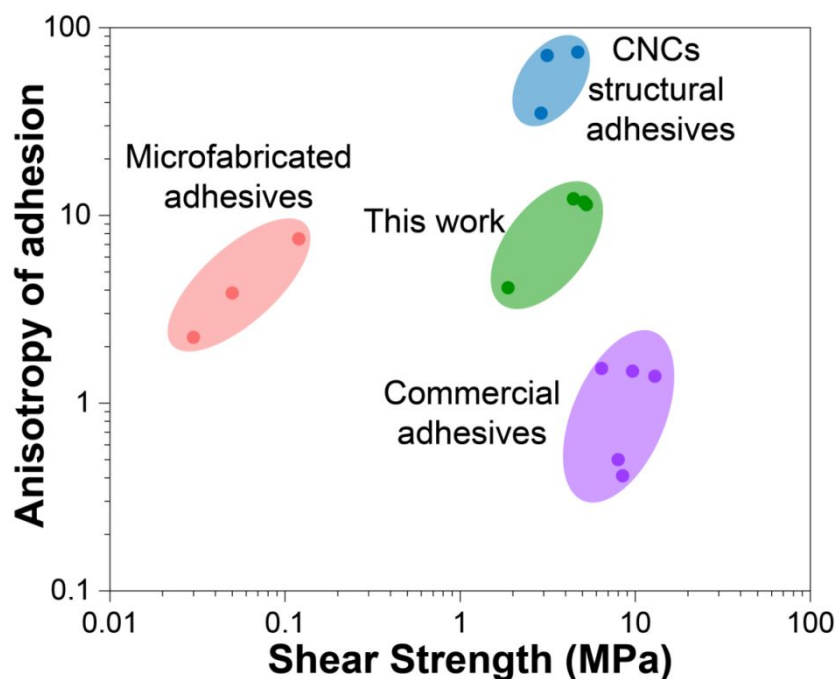


Figure S3. Anisotropy as a function of shear strength for the adhesive conditions presented in this work (green), cellulose nanocrystals (CNCs) structural adhesives (blue),¹ microfabrication approaches (pink),²⁻⁴ commercial glues such as those based on epoxy or methacrylate (purple).⁵⁻⁸

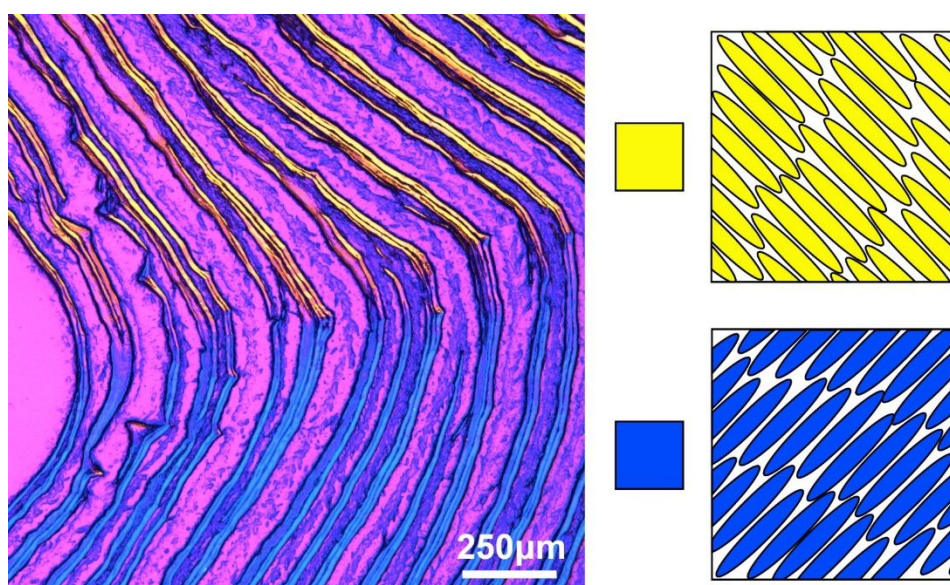


Figure S4. ChNCs adhesive layers and corresponding lamellae observed between cross polarizers with an additional retardation plate (first order wave plate, 530 nm). Yellow colors indicate top-left to bottom-right orientation and blue indicate an in-plane, orthogonal orientation to yellow colored stripe.

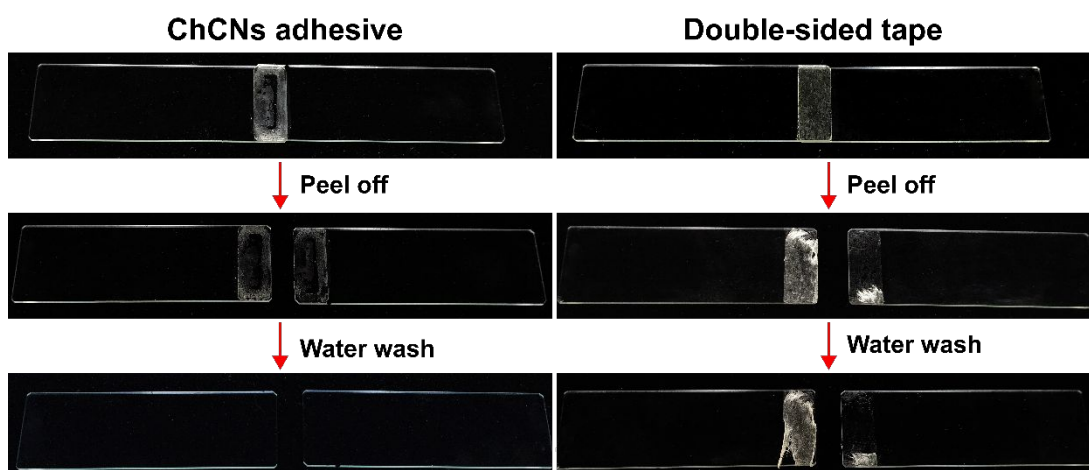


Figure S5. Photos of ChNCs nanoglue and double-sided adhesive before and after washing.

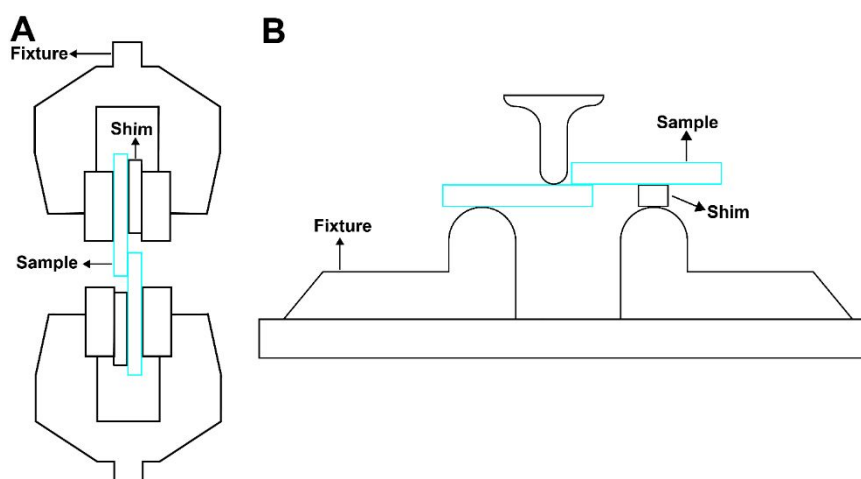
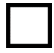






Figure S6. Illustration of adhesion strength test methods. (A) Lap-shear test. (B) Out-of-plane test.

Supplementary Table

Table S1. Adhesion failures of cardboards with different shapes glued by ChNCs adhesive.

| Substrate 1 | Substrate 2 | Weight ChNCs | Substrate Shape | Critical failure of the cardboard |
|-------------|-------------|--------------|--|-----------------------------------|
| Cardboard | Cardboard | 2 mg | Square  | Y |
| Cardboard | Cardboard | 2 mg | Rectangle  | Y |
| Cardboard | Cardboard | 2 mg | Semi-circular  | Y |
| Cardboard | Cardboard | 2 mg | Triangular  | Y |
| Cardboard | Cardboard | 2 mg | U-shape  | Y |

Supplementary Movie

Movie S1. In-plane load test of the glass sample.

Movie S2. Out-of-plane load test of the glass sample.

Movie S3. Side knock test of the glass sample.

Movie S4. Front knock test of the glass sample.

Movie S5. Drop test of the glass sample.

Movie S6. The formation of bonding structure.

References

- (1) Tardy, B. L.; Richardson, J. J.; Greca, L. G.; Guo, J.; Ejima, H.; Rojas, O. J. Exploiting Supramolecular Interactions from Polymeric Colloids for Strong Anisotropic Adhesion between Solid Surfaces. *Adv. Mater.* **2020**, *32*, 1906886.
- (2) Jeong, H. E.; Lee, J. K.; Kim, H. N.; Moon, S. H.; Suh, K. Y. A Nontransferring Dry Adhesive with Hierarchical Polymer Nanohairs. *Proc. Natl. Acad. Sci. USA* **2009**, *106*, 5639-44.
- (3) Brodoceanu, D.; Bauer, C.; Kroner, E.; Arzt, E.; Kraus, T. Hierarchical Bioinspired Adhesive Surfaces—A Review. *Bioinspir. Biomim.* **2016**, *11*, 051001.
- (4) Naito, K.; Onta, M.; Kogo, Y. The Effect of Adhesive Thickness on Tensile and Shear Strength of Polyimide Adhesive. *Int. J. Adhes. Adhes.* **2012**, *36*, 77-85.
- (5) Kaaden, C.; Powers, J. M.; Friedl, K. H.; Schmalz, G. Bond Strength of Self-Etching Adhesives to Dental Hard Tissues. *Clin. Oral Investig.* **2002**, *6*, 155-160.
- (6) Uehara, K.; Sakurai, M. Bonding Strength of Adhesives and Surface Roughness of Joined

Parts. *J. Mater. Process. Technol.* **2002**, *127*, 178-181.

(7) da Silva, L. F. M.; Rodrigues, T. N. S. S.; Figueiredo, M. A. V.; de Moura, M. F. S. F.; Chousal, J. A. G. Effect of Adhesive Type and Thickness on the Lap Shear Strength. *J. Adhes.* **2006**, *82*, 1091-1115.

(8) Badulescu, C.; Cognard, J. Y.; Créac'hcadec, R.; Vedrine, P. Analysis of The Low Temperature-Dependent Behaviour of A Ductile Adhesive Under Monotonic Tensile/Compression–Shear Loads. *Int. J. Adhes. Adhes.* **2012**, *36*, 56-64.